PCCP

ROYAL SOCIETY OF CHEMISTRY

PAPER

View Article Online
View Journal

Cite this: DOI: 10.1039/d6cp00347h

Anti-Kasha emission in DCM-IFC: computational evaluation of the type III separated wavefunction hypothesis

Pratip Chakraborty, * James N. Bull, Stephen R. Meech * and Garth A. Jones *

Kasha's rule, which states that the emitting electronic level of a given multiplicity is the lowest excited level of that multiplicity, is central to the understanding of photochemistry, and the exception due to a large (S_1–S_2) energy gap, exemplified by azulene, is well understood. Over the last few years, examples of large flexible molecules with modest (S_1–S_2) energy gaps have been reported to show anti-Kasha (AK) emission, and have been rationalised on the basis of highly spatially separated wavefunctions of the two states. Recently, a fluorophore, having such characteristics, was constructed from dicyanomethylene-4*H*-pyran (DCM) and integrated fluorescein–chromene (IFC), where a spirolactane open/closed switch was shown to regulate AK behaviour. The open form of the molecule illustrated dual emission which was interpreted as emission from both S_1 and S_2 states. Here, we investigate theoretically both the FC region and the interpolated pathways towards S_2/S_1-intersection region using implicit solvation. We calculate excited state energies and oscillator strengths employing both time-dependent density functional theory (with a range of functionals) and high-level wavefunction theories, characterising that the S_1 state is the brighter of the valence excited states, dominated by locally excited character, whereas the S_2 state is of charge-transfer character and is darker in comparison. Our *ab initio* calculations indicate that the spectral absorption profiles for the two states overlap, and that there are barrierless internal conversion pathways from the FC region on the S_2 surface towards the S_2/S_1-intersection region, which is consistent with efficient and rapid S_2 population decay in this molecule making AK emission less likely. Moreover, energy difference between S_1 and S_2 states at each of the S_1 and S_2 excited state minima is unlikely to favour thermal equilibration of population at timescales relevant to emission. Taken together, the present calculations suggest that the experimentally observed anomalous emission requires an alternative interpretation.

Received 30th January 2026,
Accepted 12th May 2026

DOI: 10.1039/d6cp00347h

rsc.li/pccp

1 Introduction

Kasha's rule, in its simplest form, states that the emitting electronic level of a given multiplicity is the lowest excited level of that multiplicity.[1] Rules are, however, not laws. Kasha and his co-workers already discovered that azulene is an exception to the rule due to a strong anomalous emission from the S_2 state.[1,2] Advances in theoretical methods and experimental techniques that are capable of following photoinduced molecular dynamics continue to demonstrate several violations of the Kasha rule.[3–34] The net result is that there are a range of molecules for which anti-Kasha (AK) behaviour has been proposed, which are reviewed in ref. 35–38. However, controversies exist as to what is interpreted as AK behaviour in certain systems, and whether impurities and/or inhomogeneity in the sample (*e.g.* multiple or distribution of ground state conformers) or artifacts in the experimental measurement have led to wrong assignments of AK behaviour.[37] This is where quantum chemical computations[39–41] can play a key role in unraveling the origin of such behaviour, or suggest its absence by explicitly investigating mechanisms for decay from higher excited states.

Recently, Veys *et al.*, with the help of detailed quantum chemical calculations in the gas phase, have categorised AK molecules into three classes depending on the role of electron-vibrational coupling.[38] Type I AK compounds consist of azulene-like molecules (*e.g.* many derivatives of azulene,cycl[3.3.3]azine)[4,5] that have a large energy gap (>1.0 eV) between the S_1 and S_2 states. This large energy gap is assumed to be the origin of anomalous emission from S_2, as it inhibits the S_2/S_1 internal conversion (IC) making radiative emission from S_2 kinetically competitive with IC. Type II AK compounds consist of molecules where the (S_2–S_1) energy gap is very small, of the

School of Chemistry, Pharmacy and Pharmacology, University of East Anglia, Norwich NR4 7TJ, UK. E-mail: p.chakraborty@uea.ac.uk, s.meech@uea.ac.uk, garth.jones@uea.ac.uk

order of k_BT, allowing for thermal repopulation of the S_2 state after IC to S_1. Examples of type II AK compounds are pyrene[24,32] and benzopyrene.[6] Types I and II AK compounds fall into strong electronic coupling regime between S_1 and S_2, however, type I has weak vibrational coupling, whilst type II has strong vibrational coupling. Nonetheless, there is another class of AK molecules that is not characterised by a large energy gap of (S_2–S_1) or thermal equilibrium of the population between the S_1 and S_2 states, and does not fit the traditional AK picture. Type III AK compounds consist of molecules characterised by the weak non-adiabatic coupling regime as the S_1 and S_2 wavefunctions are highly spatially separated. Demonstrating AK behaviour in such systems would have important implications for photonics and photochemistry. For instance, a much wider energy range of excited states could be exploited for electron injection in photovoltaic cells, and higher triplet states might be employed as sources for thermally activated delayed fluorescence, as utilised in light emitting diodes. One such type of compound is the coumarin-pyranone dyad system, the first ratiometric fluorescent probe that can reversibly detect intracellular hydropersulfide levels in living cells.[42] Recent quantum dynamical simulations of this dyad system,[43] however, show that the decay of S_2 state occurs in ~150 fs, two orders of magnitude faster than calculated in ref. 38, assuming Förster resonance energy transfer. Not long ago, several other Type III AK systems having the same building block have been claimed to illustrate AK behaviour and proposed as fluorescent probes.[22] The present study is concerned with understanding the origin and mechanism of such behaviour in these type III AK compounds, especially, in the common building block of such systems.

The aforementioned common molecular building block that falls into type III AK systems, consists of a dicynomethylene-4*H*-pyran (DCM) and an integrated fluorescein with chromene (IFC) chromophores. Although the DCM and IFC units individually illustrate conventional Kasha-like behaviour, the DCM-IFC fluorophores (see Fig. 1) have been proposed to exhibit an unusual dual emission, regulated *via* a spirolactane open/closed switch, discovered by Shi *et al.*[22] The near-infrared emission signal with maximum response at 700 nm (interpreted to arise from S_1) from DCM-IFC remains nearly constant, whilst the emission signal at 520 nm (interpreted to arise from S_2) shows a monotonic increase with analyte concentration for the open form. The aforementioned emissions were excitation-dependent and the dual emission was also claimed to not stem from impurities or molecular aggregations. Femtosecond transient absorption spectroscopy was interpreted to show a picosecond lifetime internal conversion between S_2 and S_1, whilst the S_2 state survived for ~45 ps.[22] This is much faster than the typical radiative lifetime of spontaneous emission,[1] but much longer than a typical S_2 lifetime. In a subsequent article by some of the same authors, transient absorption along with with tunable blue-side femtosecond simulated Raman spectroscopy was performed, which was interpreted to propose a S_2/S_1 internal conversion lifetime of ~1.3 ps with hydrogen out-of-plane modes influencing the internal conversion rate.[44] Thus, it was proposed that S_2 emission can compete with internal

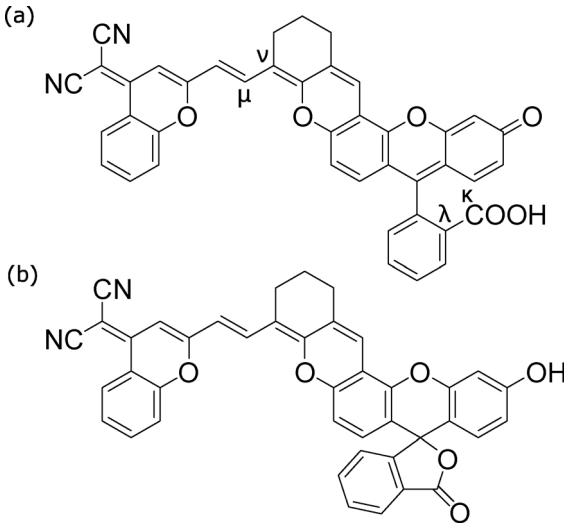

Fig. 1 Molecular structure of DCM-IFC: (a) open form – was proposed to show AK behaviour, and (b) closed form – not proposed to show AK behaviour. Torsions along C_κ–C_λ and C_μ–C_ν bonds are relevant to reach conical intersection region (see Section 3.2).

conversion between the S_2 and S_1 states. However, assuming an exponential decay with a lifetime of 1 ps (or 1.3 ps), only 36.8% of the initial population will remain in the S_2 state by 1 ps (or 1.3 ps), the majority already reaching the S_1 state; there will be no S_2 state population after 10 ps. Thus, it is difficult to rationalise how a non-negligible S_2 fluorescence signal could arise from a state with an estimated emission lifetime of ~45 ps. Moreover, the (S_2–S_1) state energy difference at the respective geometric minima was calculated to be 0.74 eV, a gap that has been claimed to suppress internal conversion between the two states. However, such a gap was demonstrated to be much larger (>1.0 eV) in azulene and its derivatives (type I), which are prototypical AK emitters.[38] Since the energy gap law is an exponential function of the gap, a change from 0.74 to 1.0 eV or more constitutes a large effect. Furthermore, from a purely potential energy surface (PES) perspective, not only the energy gap, but a large barrier in accessing the conical intersection region between the S_2 and S_1 states is critical, resulting in a competition between the IC and any AK emission from the S_2 state.

In this paper, we have used time-dependent density functional theory (TD-DFT) and single- and multireference electronic structure calculations to investigate whether AK emission is possible in DCM-IFC (open form). Inspired by the words of Sir Arthur Conan Doyle (“When you have eliminated all which is impossible, then whatever remains, however improbable, must be the truth”), we explored several possible situations that could result in AK emission. Our calculations and analysis indicate that AK emission is unlikely in the open form DCM-IFC, with implications that this may be the case for several similar type III compounds.

2 Computational methods

The ground state (S_0) of the neutral and anionic (deprotonated) form of DCM-IFC (open) were optimised using DFT[45,46] at the

M06-2X[47]/def2-SVP[48,49] level of theory using the solvation model based on density (SMD)[50] within PCM (polarizable continuum model)[51] implicit solvation *via* integral equation formalism[52–54] using water as the solvent in a similar vein to in ref. 22. Similarly, geometry optimisations were performed using TD-DFT on the first (S_1) and second (S_2) excited states of both neutral and anion form, and were confirmed to represent potential energy minima through vibrational frequency analysis. The S_0 state geometry optimisation was also performed at the M06-2X/def2-TZVP/SMD (water), ωB97X-D[55]/6-31G(d)[56,57]/PCM (water) and CAM-B3LYP[58]/6-31G(d)/PCM (water) level for an overall comparison across DFT functionals, basis sets and the implicit solvation models. Vertical excitation energies (VEEs) and oscillator strengths (*f*) were calculated for the first two excited states at the S_0 state optimised geometry at TD-DFT[59–61] level of theory using all the functionals mentioned before for both neutral and anionic forms. The VEE calculations were also improved using the corrected linear response[62] (cLR) approach implemented in Gaussian16[63] at M06-2X/def2-SVP/SMD (water) level to ensure the ordering of states at the Franck–Condon (FC) region. Moreover, the VEE and oscillator strength calculations were repeated at the single reference density-fitted second-order coupled-cluster[64] (CC2) level using Dunning basis sets[65] cc-pVDZ and cc-pVTZ and the PCM (water) model and at the multi-reference N-electron valence state perturbation theory[66–69] (NEVPT2) level based on a four-state averaged (SA4) complete active space of 8 electrons in 7 orbitals (CAS (8,7)) with the cc-pVDZ basis set and CPCM (conductor-like polarizable continuum model)[70] (water) model to ensure the validity of the TD-DFT functionals. The CC2 and NEVPT2 excited state calculations were performed using the S_0 state optimised geometry (FC geometry) obtained at the M06-2X/def2-SVP/SMD (water) level.

For absorption spectrum simulations, we employed quantum thermostat *ab initio* molecular dynamics (QT-AIMD),[71,72] as recently proposed,[73,74] to sample the ground state at a higher accuracy than harmonic Wigner sampling (harmonic sampling cannot treat low frequency anharmonic degrees of freedom) and AIMD with classical thermostats (does not include zero-point energy of a molecule). QT-AIMD helps address the limitations of both harmonic sampling and classical thermostat AIMD. QT-AIMD was performed at the DFT level using M06-2X/def2-SVP method with water as solvent within SMD model in PCM. The QT-AIMD trajectories were initiated from the corresponding optimised geometries of the neutral and anion, with velocities drawn from a Boltzmann distribution. A time step of ~0.48 fs (20 a.u.) and QT parameters (GLE drift and diffusion matrices A and C) from the GLE4MD database,[75] corresponding to a temperature of 298.15 K, N_s = 6 (additional degrees of freedom), and $\hbar\omega_{max}/k_BT$ = 20 (strong-coupling regime). For T = 298.15 K, ω_{max} = 4114.5 cm^{-1}, and exceeds the highest-frequency normal mode for DCM-IFC (open). We determined the equilibration time of the trajectories by monitoring the convergence of the average kinetic energy.[74] From the thermalised trajectories, we extracted 105 samples (every ~20 fs) for both the neutral and anion of DCM-IFC (open). VEEs and oscillator strengths were calculated for S_1 and S_2 states at M06-2X/def2-SVP level with SMD (water) model and the VEEs were improved *via* the cLR approach. The resultant stick spectra from the VEEs and oscillator strengths of S_1 and S_2 states were convolved with a Gaussian (FWHM = 0.2 eV) to generate absorption spectra for both the neutral and the anionic DCM-IFC (open). All QT-AIMD simulations were carried out using the ABIN code[76] interfaced with Gaussian16[63] for the electronic-structure calculations. In addition, ground state classical thermostat AIMD were also performed for both neutral and anionic DCM-IFC (open) using M06-2X/def2-SVP method with water as solvent within SMD model in CPCM, thermalised at 298.15 K using ORCA 5.0.4,[77] for a comparison with the QT-AIMD generated absorption spectra. 50 independent snapshots (every 20 fs) were collected from the equilibrated AIMD trajectories for both neutral and anionic DCM-IFC (open). VEE and oscillator strengths were calculated for S_1 and S_2 states at the same level of theory as was done for QT-AIMD sampled geometries and the same FWHM was used for absorption spectrum simulation. Excited state sampling was also performed for S_1 and S_2 states using QT-AIMD for both neutral and anion of DCM-IFC (open), at the TD-DFT level, using the same functional, basis set, implicit solvation model and same QT parameters, as employed in the ground state QT-AIMD. These QT-AIMD trajectories were initiated from the corresponding excited state optimised geometries at the TD-DFT level. For a detailed discussion of the importance of sampling initial conditions with QT-AIMD, the reader is referred elsewhere.[74,78]

Optimisation of the minimum-energy conical intersection between S_2 and S_1 was attempted at the level of TD-DFT with Tamm–Dancoff approximation[79] (TDA) using CAM-B3LYP/6-31G(d) with the CPCM (water) method in ORCA 5.0.4. Geometries with electronic degeneracies (not converged, but with energy difference between S_2 and S_1 of 0.036 eV for neutral and 0.013 eV for anion) were found for DCM-IFC (open). Linear interpolations were carried out in internal coordinates (LIIC) between FC geometry (optimised at M06-2X/def2-SVP/SMD (water)) and the above-mentioned geometries with electronic degeneracy. PESs were constructed along such LIIC at TD-DFT/M06-2X/def2-SVP/SMD(water), CC2/cc-pVDZ/PCM(water) and NEVPT2/SA4-CAS(8,7)/cc-pVDZ/CPCM(water). LIICs were also constructed between S_2 optimised geometries and the above-mentioned geometries with electronic degeneracy, for both neutral and anion, with PES calculated at TD-DFT/M06-2X/def2-SVP/SMD(water) level.

TD-DFT, CC2 and NEVPT2 single point calculations were performed using Gaussian16,[63] MRCC[80,81] and ORCA5.0.4[77] packages, respectively.

3 Results and discussions

3.1 Does 480 nm pump excite the S_2 state?

Shi *et al.* excited the open form of DCM-IFC at 480 nm (2.58 eV) and the closed form of DCM-IFC at 560 nm (2.21 eV).[22] Excitation of the open form has been proposed to lead to dual

emission at 520 (2.38 eV) and 700 nm (1.77 eV), with emission at 520 nm interpreted to be of AK origin. According to their S_1 and S_2 state geometry optimisations at TD-M06-2X/def2-SVP/SMD(water) level, these observed emission bands correspond to the energy difference between S_1 and S_0, and S_2 and S_0, at the S_1 and S_2 state minima, respectively. The VEEs for S_2 and S_1 at the FC region was reported to lie in the region of 485 nm and 563 nm based on the optimised geometry and energy calculated at (TD)-PBE0/6-311+G(d,p)/PCM level.[44] Natural transition orbital calculations[22] at both the minima illustrate that the $S_0 \rightarrow S_1$ transition corresponds to a locally excited state (electron and hole being on the same part of the chromophore) and $S_0 \rightarrow S_2$ transition corresponds to a charge-transfer state (electron and hole being on different parts of the chromophore). Nonetheless, a locally excited state is generally the bright state with high oscillator strength due to high degree of spatial overlap of molecular orbitals, whilst a charge-transfer state has a low oscillator strength due to low degree of spatial overlap of molecular orbitals. If the transitions correspond to the same character at the FC region, that would lead to S_1 being a bright state and S_2 being a comparatively darker state. Hence, it becomes important to investigate which state is excited in DCM-IFC (open) *via* a 480 nm pulse, before exploring whether AK emission can be realised in this molecule.

3.1.1 Vertical excitation energies and oscillator strengths. In solution, DCM-IFC(open) can exist both as neutral and anion depending on the pH of the buffer (although at low pH, it exists as the closed form). We have thus calculated the VEEs and oscillator strengths of both neutral and anion forms using TD-DFT method with several functionals and also using high-level density-fitted CC2 theory. The hybrid meta generalised gradient approximation (GGA) funtional, M06-2X was originally used in ref. 22, and performs well for charge-transfer states because it includes high exact exchange.[82] We use the M06-2X functional and compare it to range-separated hybrid functionals (CAM-B3LYP and ωB97X-D) that are designed to treat charge-transfer states more rigorously.[83–86] All of these calculations have been performed using implicit solvation models, as shown in Tables 1 and 2. In these models, the excited states are calculated in presence of solvent polarisation for the ground state *via* linear response formalism. The specific excited states can then be relaxed to equilibrate with respect to the solvent field.[62] Such state-specific corrections have been attempted using the cLR approach to ensure the ordering of the excited states at the FC region.

Levels of theory across different functionals, basis sets and implicit solvents, unanimously show that S_1 is the brighter of the two states, by an order of magnitude, for both neutral and anionic forms of DCM-IFC (open). This is also illustrated by dominant orbital contributions at TD-DFT level (shown in Fig. 2) where the $S_0 \rightarrow S_1$ transition corresponds to local excitation and the $S_0 \rightarrow S_2$ transition has charge-transfer character. In addition, the excitation wavelength used in ref. 22, 480 nm (2.58 eV) also corresponds to the locally excited S_1 state for all calculations. The charge-transfer S_2 state is located approximately 0.5–0.6 eV higher in energy compared to the S_1 state at the FC region using TD-DFT functionals and linear response implicit solvation. The same behaviour was also found at the CC2 level. The cLR formalism demonstrates that the gap between S_2 and S_1 states drop from 0.50 eV in neutral and 0.58 eV in anion (ground state solvation) to 0.22 eV in neutral and 0.39 eV in anion, although the ordering remains the same at the FC region. Our VEE calculations with several methods do not correspond to the VEEs calculated at the PBE0 level (used in ref. 44), and thus we utilise TD-M06-2X level from here on. We note that hybrid GGA functionals such as PBE0 can overstabilise charge-transfer states.[87] For completeness, we also performed TDA VEE calculations at the M06-2X/def2-SVP/SMD (water) level, which yield excitation energies that are slightly blue shifted ($\sim$0.1 eV) relative to TD-DFT at the same level, but do not affect the state ordering (see Tables S1 and S2 in the SI).

Table 1 DCM-IFC (open) neutral: VEEs and oscillator strengths (f) associated with the lowest two excited states using implicit solvation models

Method	State	Energy (eV)	f
TD-M06-2X/def2-SVP/SMD (water)	S_1	2.552	2.06
	S_2	3.050	0.17
TD-CAM-B3LYP/6-31G(d)/PCM (water)	S_1	2.629	2.11
	S_2	3.243	0.28
TD-ωB97x-D/6-31G(d)/PCM (water)	S_1	2.668	2.17
	S_2	3.308	0.36
TD-M06-2X/def2-TZVP/SMD (water)	S_1	2.489	2.03
	S_2	3.013	0.19
CC2/cc-pVDZ/PCM (water)[a]	S_1	2.591	2.67
	S_2	2.976	0.61
CC2/cc-pVTZ/PCM (water)[a]	S_1	2.486	2.57
	S_2	2.861	0.64
TD-M06-2X/def2-SVP/cLR-SMD (water)	S_1	2.614	2.06
	S_2	2.838	0.17

[a] CC2 VEEs were calculated at the structure optimised using M06-2X/def2-SVP level with SMD (water) and the respective oscillator strengths were obtained using configuration interaction singles (CIS) wavefunctions. For the cLR approach, only the VEEs are corrected and the oscillator strengths were taken from the linear response approach.

Table 2 DCM-IFC (open) anion: VEEs and oscillator strengths (f) associated with the lowest two excited states using implicit solvation models

Method	State	Energy (eV)	f
TD-M06-2X/def2-SVP/SMD (water)	S_1	2.539	2.01
	S_2	3.119	0.23
TD-CAM-B3LYP/6-31G(d)/PCM (water)	S_1	2.601	2.03
	S_2	3.330	0.42
TD-ωB97x-D/6-31G(d)/PCM (water)	S_1	2.642	2.08
	S_2	3.352	0.42
TD-M06-2X/def2-TZVP/SMD (water)	S_1	2.525	2.05
	S_2	3.034	0.19
CC2/cc-pVDZ/PCM (water)[a]	S_1	2.559	2.59
	S_2	3.087	0.67
CC2/cc-pVTZ/PCM (water)[a]	S_1	2.456	2.51
	S_2	2.961	0.68
TD-M06-2X/def2-SVP/cLR-SMD (water)	S_1	2.560	2.01
	S_2	2.953	0.23

[a] CC2 VEEs were calculated at the structure optimised using M06-2X/def2-SVP level with SMD (water) and the respective oscillator strengths were obtained using CIS wavefunctions. For the cLR approach, only the VEEs are corrected and the oscillator strengths were taken from the linear response approach.

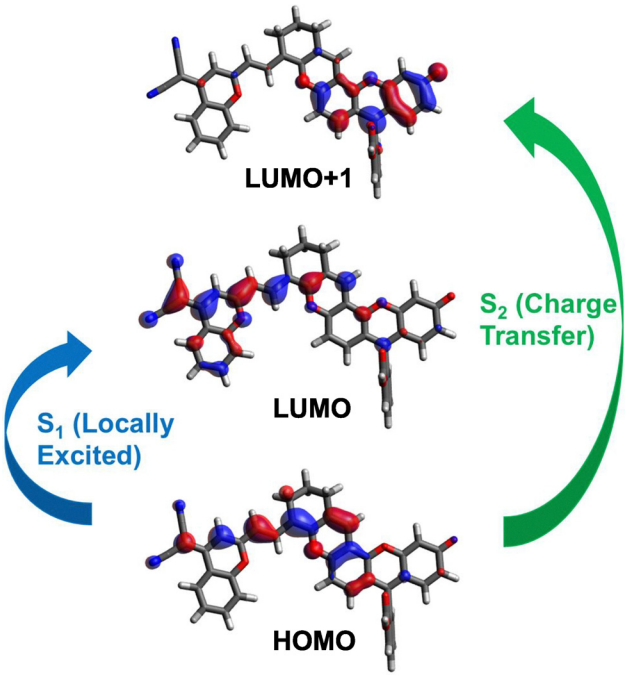

Fig. 2 Dominant orbital excitations associated with the lowest two excited electronic states of the neutral form DCM-IFC (open) at TD-M06-2X/def2-SVP level with SMD (water) model. Isovalue = 0.03 a.u. The same orbital excitations are observed for the two excitations of the anionic form. NTOs for both neutral and anion form are also available in the SI, demonstrating the same characters.

The VEEs and oscillator strengths of the states indicate that the S_1 state will have much higher absorption cross section compared to the S_2 state, and there is much higher probability that population will be promoted to the S_1 state with a 480 nm pulse. Inclusion of an empirical redshift of 0.3–0.5 eV allows for population to be excited to either the S_2 states or a mix of S_1 and S_2 states.

3.1.2 Simulated absorption spectra. The simulated absorption spectra for neutral and anionic DCM-IFC (open) determined by calculating VEEs (corrected using the cLR formalism) and oscillator strengths at TD-M06-2X/def2-SVP level with SMD (water) model, from QT-AIMD sampling, are shown in Fig. 3. The neutral and the anion spectra have been compared to the experimental absorption spectrum of the DCM-IFC-ester available in ref. 22, and anionic DCM-IFC (open) avalable in ref. 44, respectively. The theoretical spectra were redshifted by 0.17 and 0.16 eV for the neutral and the anion, respectively, to match the experimental maximum. The S_2 contribution to the spectrum arises as a shoulder on the neutral DCM-IFC spectrum and as a small peak on the anionic DCM-IFC spectrum, which is in accordance with the energy difference between S_1 and S_2 at the FC region, with S_2 being blue-shifted for the anionic form compared to the neutral form. Benchmarking of theoretical methods has shown that absorption maximum or VEEs calculated *via* TD-DFT typically overestimate the experimental absorption maximum by 0.2–0.5 eV.[82,83,88] This overestimation depends on several aspects such as which functional and/or basis set is used and whether solvation is employed or not.

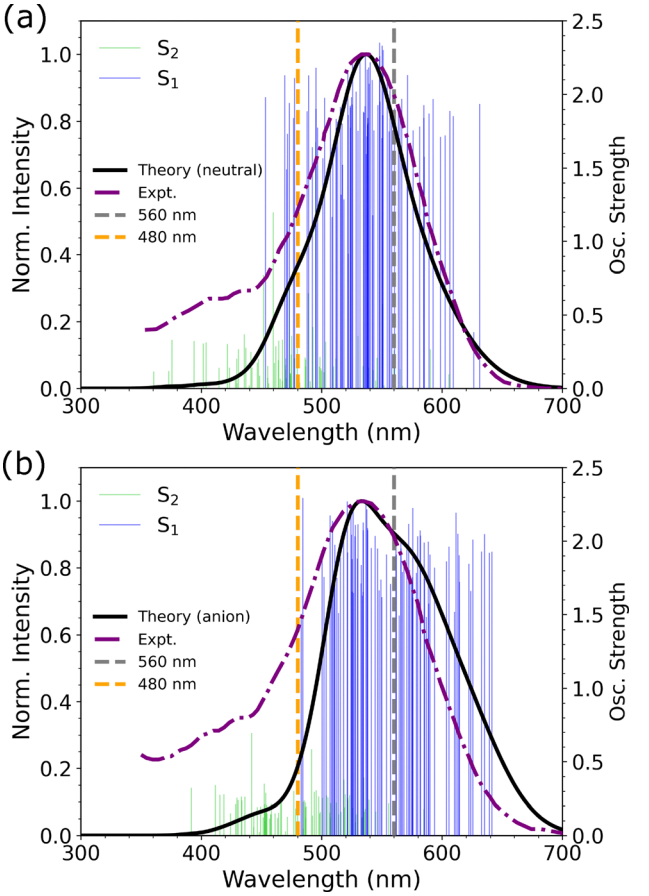

Fig. 3 Absorption spectra of the (a) neutral form and the (b) anion form of DCM-IFC (open) simulated from calculating VEEs and oscillator strengths at TD-M06-2X/def2-SVP/SMD (water) level with geometries sampled from QT-AIMD. VEEs were updated using the cLR formalism. The resultant stick spectra were convolved with a Gaussian with FWHM of 0.2 eV and uniformly redshifted by 0.17 and 0.16 eV for the neutral and the anion to match with the experimental absorption maximum of DCM-IFC-ester (open) (digitised and normalised from ref. 22) and anionic DCM-IFC (open) (digitised and normalised from ref. 44), respectively.

Typically, with range-separated functionals along with implicit solvation models, such shifts are smaller, especially for charge-transfer states. We have shown that the VEEs and oscillator strengths calculated using the M06-2X functional for this system are very similar to those determined with the range-separated hybrid functionals. The empirical shift that we have implemented here (0.17 and 0.16 eV) is consistent with the literature value of overestimation of VEEs.[82,83,88] The agreement suggests that a 480 nm pulse will excite population to the S_2 state (or excite population to both states). The absorption spectrum simulated after ground state sampling *via* classical thermostat AIMD (see Fig. S3 of the SI), whilst narrower due to the absence of zero-point energy, allows us to conclude the same. The QT-AIMD generated anion absorption spectrum also has a vibrational structure that is not resolved in the experimental absorption spectrum and also not captured in the spectrum generated *via* classical thermostat AIMD. The S_1 sticks show a progression of $\sim$0.2 eV ($\sim$1613 cm^{-1}), indicating that C=C stretching modes are responsible for this vibrational

structure. To understand the fate of the excited population on S_2, we investigate whether S_2 is stable and therefore potentially emissive, or whether there are barrierless pathways that exist from the FC region towards S_2/S_1 conical intersection.

3.2 Is there a barrier in accessing the S_2/S_1 intersection region?

Our attempts at conical intersection optimisation between S_2 and S_1 have suggested two types of intersection. For the neutral form, we have found an intersection region where the main backbone of the molecule stays planar (no torsion along C_μ–C_ν), but there is a substantial torsion (θ) of the C–C (C_λ–C_κ) bond (Fig. 1(a)) connecting the COOH group and the dangling phenyl ring. In addition, another intersection region has been located for the anion which is mainly characterised by a substantial torsion (ϕ) (along C_μ–C_ν) (Fig. 1(a)) of the two main units of the molecule along with a torsion (θ) of the C_λ–C_κ bond. Since this molecule has $\geq$210 (213 for neutral and 210 for anion) vibrational degrees of freedom, it is expected that there will be S_2/S_1-intersections along several other dimensions. Even for smaller organic molecules, several conical intersection regions with distinct nuclear motions are located, and are usually exemplified when conducting non-adiabatic dynamics simulations.[78,89–92] Locating additional intersection regions, thus, becomes irrelevant in the present case. Instead, the crucial question is whether there are barrierless pathways that exist along any such intersection from the FC region. The presence of barrierless access to S_2/S_1-intersection from FC region is expected to facilitate efficient population transfer from S_2 to S_1, in ultrafast (ps or sub-ps) manner, thereby limiting significant fluorescence from S_2.

Our calculations identified such barrierless pathways for both neutral and anion forms, as shown in Fig. 4 and 5, respectively, from the FC region towards the intersection region at all tested levels of theory. A general trend that can be observed (especially from Tables 1 and 2) is that the S_2 state is slightly overestimated at the TD-M06-2X level compared to higher level electronic structure methods CC2 and NEVPT2 (and TD-M06-2X level with cLR approach), and thus, the intersection lies substantially closer to the FC region at higher levels of theory compared to TD-M06-2X. The mass-weighted distance illustrates that the S_2/S_1-intersection region is structurally much closer to the FC region for the neutral compared to the anion (associated with the torsion of around the C_μ–C_ν bond). In addition, PES along LIICs between S_2 minimum geometry and the S_2/S_1-intersection region (see Fig. S4 and S5 in the SI), show that the S_1 and S_2 states are in close proximity to each other along the LIIC. Even though a portion of the excited population may traverse towards the S_2 minimum and has a slightly uphill pathway of $\leq$0.02 eV (negligible) and $\leq$0.23 eV to reach the intersection from the S_2 minimum, for the neutral and anion, respectively, such small energetic increases are not consistent with S_2 population decay of the order of $\sim$45 ps. As discussed above, presence of no barrier towards the intersection region from the FC region suggests efficient population transfer from S_2 to S_1, on timescales comparable to the $\sim$1 ps time constant interpreted as internal conversion from S_2 to S_1 in DCM-IFC (open).[22,44]

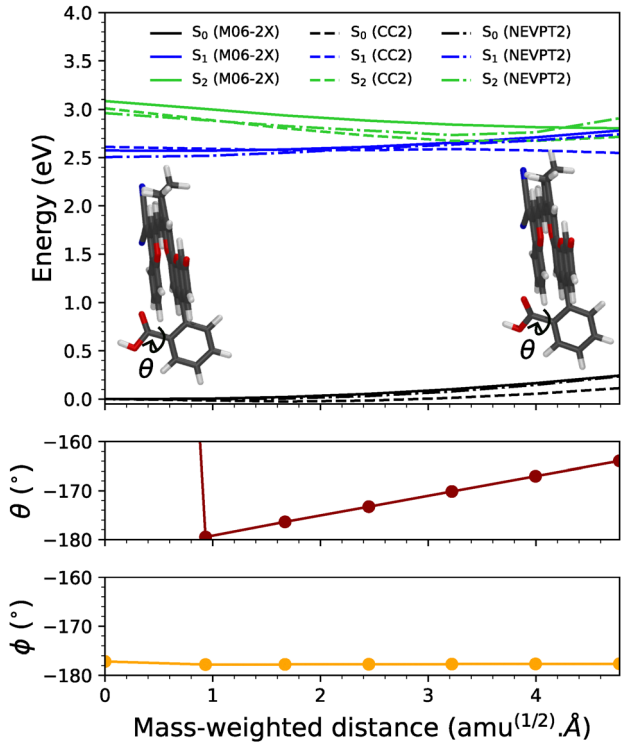

Fig. 4 Relative energies (top panel) along LIIC pathways from the FC region to S_2/S_1 intersection region for the neutral DCM-IFC (open) with the important torsions (dihedral angles) θ (middle panel) and ϕ (bottom panel) along the same LIIC. Energies are calculated relative to the ground state energy at each level of theory at the FC geometry. The θ value for the first LIIC point falls on the positive side of 180° showing a jump in θ between first and second point of the LIIC. However, the difference in θ between these two points is only 3°.

3.3 Is thermal equilibration possible on the excited-state manifold?

As shown in Tables 3 and 4, the emission energies calculated at the S_1 and S_2 state equilibrium geometries are 1.758 eV (705.3 nm) and 2.419 eV (512.5 nm) for the neutral and 1.755 eV (706.4 nm) and 2.494 eV (497.1 nm) for the anion, respectively. These emission energies agree with the experimental emission reported by Shi *et al.*[22] at 520 and 700 nm, as is also demonstrated in their paper with the calculated values for the anionic form at the exact same level of theory. However, the agreement between the experimental and theoretical emission energies is coincidental. The aforementioned emission energies are calculated using the ground state solvent reaction field, whilst emission ensues from the excited state minimum. Thus, emission energy should be calculated in the solvent reaction field that is created in response to the specific excited state charge distribution. Like before, we use the cLR formalism to calculate the emission energies. This illustrates that the S_1 and S_2 emission energies are at 2.223 eV (557.7 nm) and 2.304 eV (538.1 nm) for the neutral and at 2.219 eV (558.7 nm)

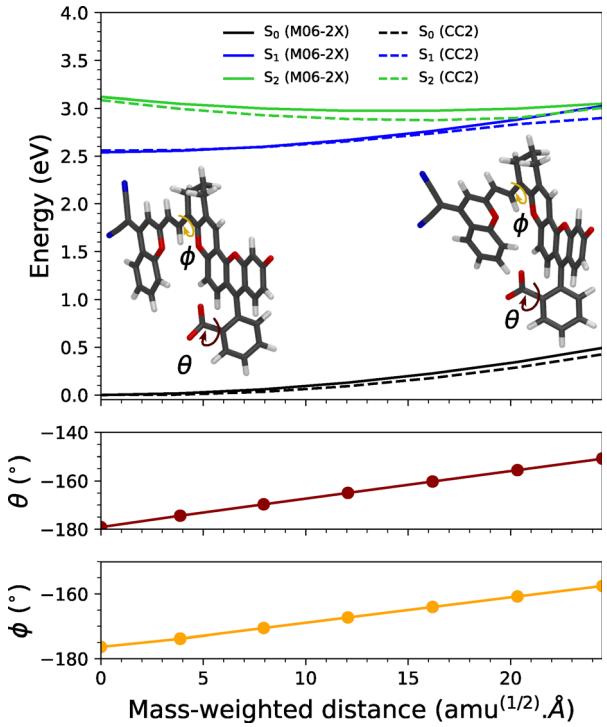

Fig. 5 Relative energies (top panel) along LIIC pathways from the FC region to S_2/S_1 intersection region for the anionic DCM-IFC (open) with the important torsions (dihedral angles) θ (middle panel) and ϕ (bottom panel) along the same LIIC. Energies are calculated relative to the ground state energy at each level of theory at the FC geometry.

Table 3 Calculated emission energies for neutral DCM-IFC (open)

Method	Emission state	Emission energy (eV)	ΔE (eV)
TD-M06-2X/def2-SVP/ SMD(water)	S_1	1.758	0.661
	S_2	2.419	
TD-M06-2X/def2-SVP/cLR-SMD(water)	S_1	2.223	0.081
	S_2	2.304	

Table 4 Calculated emission energies for anionic DCM-IFC (open)

Method	Emissive state	Emission energy (eV)	ΔE (eV)
TD-M06-2X/def2-SVP/ SMD(water)	S_1	1.755	0.739
	S_2	2.494	
TD-M06-2X/def2-SVP/cLR-SMD(water)	S_1	2.219	0.227
	S_2	2.446	

and 2.446 eV (506.9 nm) for the anion. Although the S_2 emission still agrees with one of the experimentally measured fluorescence peak in ref. 22, the S_1 emission does not. The difference in energy at the S_1 and S_2 minima in the ground state solvent reaction field is ~0.7 eV, which is much higher than thermal energy (0.026 eV) at the room temperature. However, the energy differences at the minima after the correction are 0.081 eV for the neutral and 0.227 eV for the anion, much closer to thermal energy at room temperature. Nonetheless, the mass-weighted distance between the S_1 and S_2 minima is large (8.171 and 9.282 amu$^{1/2}$ Å for neutral and anion, respectively), showing that the two minima correspond to distinct regions of configuration space. What is therefore most relevant is the energy difference between the excited states evaluated at S_1 and S_2 minima. Fig. S6 and S7 show that the excited state energy difference is 0.80 and 0.88 eV, much larger than thermal energy at room temperature, for neutral and anion, respectively, at the S_1 minimum. Fig. S4 and S5 show that the excited state energy difference is 0.14 and 0.21 eV, still larger than thermal energy at room temperature, for neutral and anion, respectively, at the S_2 minimum. In a non-adiabatic dynamics simulation, population may leak back to S_2 after being on S_1 momentarily, especially because of the excess vibrational energy accessed on reaching S_1 from S_2, and that the S_1 and S_2 states are close to one another with rather flat topography near the S_2/S_1-intersection (Fig. 4 and 5) and along the pathway from the S_2 minimum to the S_2/S_1-intersection (Fig. S4 and S5). This situation was observed in a non-adiabatic dynamics simulation (albeit at a semi-empirical level) for a LPPP5-PMI dyad – a system having highly spatially separated S_1 and S_2 wavefunctions like DCM-IFC (open).[93] Even then, the S_2 population decay was found to be ultrafast with a lifetime of 55 fs at 300 K, with no population left on S_2 after 300 fs. However, fluorescence typically occurs on nanosecond timescales (albeit ~45 ps for DCM-IFC(open)[22]). During such a timescale, no thermal equilibrium is expected between S_1 and S_2 with such energy differences, especially for the deprotonated (anion) form which dominates the measurement sample.[22,44] Excited state sampling using QT-AIMD also illustrate that there is no state character switching at the S_1 minimum, whereas state characters switch for a few sample geometries (11% and 5% for neutral and anion, respectively), leading to S_2 being brighter, at the S_2 minimum (see Fig. S8 and S9 of the SI). This, however, stems from the proximity of the two states at S_2 minimum (see Fig. S4 and S5 of the SI). Dynamically, the barrierless pathway towards the S_2/S_1-intersection region from the FC region is expected to facilitate efficient population transfer from S_2 to S_1, allowing only a small fraction of the excited population to reach the minimum of the S_2 state. Consequently, the likelihood of retaining the bright state population in S_2 is significantly reduced (*i.e.* lower than 11% and 5% for the neutral and anion), especially, for the anionic form of DCM-IFC (open).

3.4 On the limitations of the computational approach

Although the present results provide substantial evidence that challenges the previously proposed AK mechanism, we acknowledge several limitations of the computational approach. First, the inference of rapid $S_2 \rightarrow S_1$ internal conversion is based on the apparent absence of energetic barriers and the accessibility of crossing regions, rather than direct simulation of non-adiabatic molecular dynamics. In this respect, non-adiabatic molecular dynamics simulations would be required to explicitly quantify the excited-state population evolution. However, such simulations at a multiconfigurational level of theory remain

computationally prohibitive for systems of this size (210 degrees of freedom). Next, the characterisation of the S_2/S_1-intersection region relies on near-degenerate geometries obtained at the TDA level and linear interpolation paths calculated at TD-DFT level. While these provide useful insight, they do not fully capture the multidimensional nature of conical intersection seams or the associated branching space and therefore cannot uniquely define the relaxation pathway. However, we emphasise the presence of at least one barrierless pathway that is consistent with efficient population transfer from S_2 to S_1. Finally, solvent effects are treated using implicit models, which may not fully account for specific solute–solvent interactions, particularly in the presence of charge-transfer character. Despite these limitations, the consistent observation across multiple methods is (i) S_1 is brighter than S_2 in the FC region and (ii) energetically accessible pathways exist toward S_2/S_1-intersection region. Together, these observations challenge the previously proposed AK interpretation and motivates further experimental and theoretical investigation.

4 Conclusions and outlook

We have investigated the FC region and mapped the pathway towards S_2/S_1-intersection region from the FC region in the open form of DCM-IFC, a system having high degree of spatial separation between its S_1 and S_2 wavefunctions which is thus hypothesised and proposed to demonstrate AK emission. Using TD-DFT and high-level electronic structure calculations in presence of implicit solvent models, we have shown that the S_1 state, which is locally excited, is the brighter of the lower valence excited states in this molecule, and corresponds closely to the experimental laser pulse used for excitation in ref. 22, and S_2 is a charge-transfer state and is much darker in comparison. However, after employing redshifts (to match experimental absorption maxima) to the theoretical spectra of both neutral and anion, it is expected that 480 nm laser pulse will excite population to either the S_2 state or both the S_1 and S_2 states. Nonetheless, barrierless access to the S_2/S_1-intersection region from the FC region on S_2 suggests an efficient, and rapid, S_2 population decay, which is inconsistent with sustained AK emission. The energy differences between the S_1 and S_2 states at the individual S_1 and S_2 excited state minima are also larger than the thermal energy at room temperature, suggesting that thermal equilibrium between the excited states is unlikely at timescales relevant for fluorescence.

Thus, an alternative assignment for the anomalous emission may need to be considered. Although our results do not provide a definitive explanation for the experimentally observed emission, they indicate that the previously proposed AK interpretation for DCM-IFC (open) may not be supported by the underlying excited-state landscape. Our calculations indicate that the photophysics of DCM-IFC (open) is more complex than previously assumed, suggesting that spatial separation of excited state wavefunctions alone may not fully account for the observed behaviour. If this is already the case for the DCM-IFC building block, then related compounds synthesised using this motif and employed for ratiometric sensing may likewise exhibit anomalous emission originating from alternative mechanisms. Clarifying the true source of this emission is therefore crucial both for correctly interpreting existing experimental results and for guiding the rational design of future sensing architectures.

Conflicts of interest

There are no conflicts to declare.

Data availability

Supplementary information: additional LIIC pathways, NTO orbitals, active spaces employed, details of excited state sampling *via* QT-AIMD, and simulated absorption spectra *via* classical AIMD are provided. See DOI: https://doi.org/10.1039/d6cp00347h.

The Cartesian coordinates of all the critical points on the ground and excited states are provided in the electronic supplementary information (SI).

Acknowledgements

The authors acknowledge support from the Engineering and Physical Sciences Research Council (EPSRC, Award No. EP/Y021525/1). The authors thank Dr Khalid Siddiqui, Dr Claire Jones and Dr Andrew N. Cammidge for helpful discussions. PC also thanks Dr Felix Plasser and Dr Basile Curchod for helpful discussions during a conference. The calculations presented in this paper were carried out on the High-Performance Computing Cluster supported by the Research and Specialist Computing Support service and the Bull group cluster at the University of East Anglia.

References

1 M. Kasha, *Discuss. Faraday Soc.*, 1950, **9**, 14–19.
2 G. Viswanath and M. Kasha, *J. Chem. Phys.*, 1956, **24**, 574–577.
3 S. K. Behera, S. Y. Park and J. Gierschner, *Angew. Chem., Int. Ed.*, 2021, **60**, 22624–22638.
4 S. Awuku, S. J. Bradley, K. P. Ghiggino, R. P. Steer, A. L. Stevens, J. M. White and C. Yeow, *Chem. Phys. Lett.*, 2021, **784**, 139114.
5 W. Leupin and J. Wirz, *J. Am. Chem. Soc.*, 1980, **102**, 6068–6075.
6 G. Hoytink, *Chem. Phys. Lett.*, 1974, **26**, 16–19.
7 N. A. Shekhovtsov and M. B. Bushuev, *J. Photochem. Photobiol., A*, 2022, **433**, 114195.
8 D. Malpicci, E. Lucenti, C. Giannini, A. Forni, C. Botta and E. Cariati, *Molecules*, 2021, **26**, 6999.
9 D. Tong, F. Siddique, C. Qian, G. V. Baryshnikov and H. Wu, *Dyes Pigm.*, 2023, **219**, 111625.

10 N. A. Shekhovtsov, E. B. Nikolaenkova, A. S. Berezin, V. F. Plyusnin, K. A. Vinogradova, D. Y. Naumov, N. V. Pervukhina, A. Y. Tikhonov and M. B. Bushuev, *ChemPlusChem*, 2021, **86**, 1436–1441.
11 D. Malpicci, A. Forni, E. Lucenti, D. Marinotto, D. Maver, V. Lozovan, V. C. Kravtsov, A. Siminel, M. S. Fonari and E. Cariati, *Eur. J. Inorg. Chem.*, 2024, e202400338.
12 S. Gao, J. Ding, S. Yu and F. Li, *J. Mater. Chem. C*, 2023, **11**, 6400–6406.
13 J. Franz, M. Oelschlegel, J. P. Zobel, S.-A. Hua, J.-H. Borter, L. Schmid, G. Morselli, O. S. Wenger, D. Schwarzer, F. Meyer and L. González, *J. Am. Chem. Soc.*, 2024, **146**, 11272–11288.
14 V. I. Tomin and A. Wodarkiewicz, *J. Lumin.*, 2018, **198**, 220–225.
15 H. Wang, J. Wang, T. Zhang, Z. Xie, X. Zhang, H. Sun, Y. Xiao, T. Yu and W. Huang, *J. Mater. Chem. C*, 2021, **9**, 10154–10172.
16 H. Imada, M. Imai-Imada, X. Ouyang, A. Muranaka and Y. Kim, *J. Chem. Phys.*, 2022, **157**, 104302.
17 Q. Mu, K. Zhang, H. Zou, H. Liu, Y. Song, C.-K. Wang, L. Lin and J. Fan, *Dyes Pigm.*, 2022, **205**, 110560.
18 X. Zhang, C. Chen, W. Zhang, N. Yin, B. Yuan, G. Zhuang, X.-Y. Wang and P. Du, *Nat. Commun.*, 2024, **15**, 2684.
19 W. Xie, W. Huang, J. Li, Z. He, G. Huang, B. S. Li and B. Z. Tang, *Nat. Commun.*, 2023, **14**, 8098.
20 I. Sahalianov, R. R. Valiev, R. R. Ramazanov and G. Baryshnikov, *J. Phys. Chem. A*, 2024, **128**, 5138–5145.
21 N. A. Shekhovtsov, S. Vorobeva, E. B. Nikolaenkova, A. A. Ryadun, V. P. Krivopalov, C. Gourlaouen and M. B. Bushuev, *Inorg. Chem.*, 2023, **62**, 16734–16751.
22 L. Shi, C. Yan, Z. Guo, W. Chi, J. Wei, W. Liu, X. Liu, H. Tian and W.-H. Zhu, *Nat. Commun.*, 2020, **11**, 793.
23 M. Nazari Haghighi Pashaki, C. D. Bösch, F. Garo, A. Blanc, M. Marazzi, A. Rondi, M. Gazzetto, M. Akbarimoosavi, J.-C. Tremblay, S. M. Langenegger, A. Monari, R. Häner, T. Feurer and A. Cannizzo, *Angew. Chem., Int. Ed.*, 2025, **64**, e202513001.
24 G. Braun, I. Borges, A. J. A. Aquino, H. Lischka, F. Plasser, S. A. do Monte, E. Ventura, S. Mukherjee and M. Barbatti, *J. Chem. Phys.*, 2022, **157**, 154305.
25 Y. Wu, J. Zhang, S. Chen, W. Li, C. Liu, X. Mu, T. Feng, D. Chen, K. Fang, L. Wu, T. Wang and Z. Ge, *Laser Photonics Rev.*, 2024, **18**, 2400902.
26 B. H. Jhun, D. Y. Jeong, S. Nah, S. Y. Park and Y. You, *J. Mater. Chem. C*, 2021, **9**, 7083–7093.
27 P. Nag, P. Rohila and S. R. Vennapusa, *J. Photochem. Photobiol., A*, 2024, **448**, 115296.
28 Z. Zhu, Z. Kuang, L. Shen, S. Wang, X. Ai, A. Abdurahman and Q. Peng, *Angew. Chem.*, 2024, **136**, e202410552.
29 A. Georgiev, D. Yordanov, N. Vassilev, V. Deneva, D. Nedeltcheva, I. Angelov and L. Antonov, *Phys. Chem. Chem. Phys.*, 2021, **23**, 13760–13767.
30 A. Belashov, A. Zhikhoreva, S. Lermontova, T. Lyubova, L. Klapshina, I. Semenova and O. Vasyutinskii, *J. Photochem. Photobiol., A*, 2025, **458**, 115964.
31 V. M. Korshunov, T. N. Chmovzh, A. V. Tsorieva, G. A. Gruzdev, D. M. Rakhimkulov, I. V. Taydakov and O. A. Rakitin, *J. Mater. Chem. C*, 2024, **12**, 19200–19211.
32 M. d O. Bispo, R. Souza Mattos, M. J. Pinheiro, B. C. Garain, P. O. Dral and M. Barbatti, *J. Chem. Theory Comput.*, 2025, **21**, 11390–11400.
33 N. A. Shekhovtsov and M. B. Bushuev, *J. Mol. Liq.*, 2025, **425**, 127260.
34 N. A. Shekhovtsov and M. B. Bushuev, *Phys. Chem. Chem. Phys.*, 2026, **28**, 1806–1819.
35 T. Itoh, *Chem. Rev.*, 2012, **112**, 4541–4568.
36 A. P. Demchenko, V. I. Tomin and P.-T. Chou, *Chem. Rev.*, 2017, **117**, 13353–13381.
37 J. C. Del Valle and J. Catalán, *Phys. Chem. Chem. Phys.*, 2019, **21**, 10061–10069.
38 K. Veys and D. Escudero, *Acc. Chem. Res.*, 2022, **55**, 2698–2707.
39 X. Zhang, D. Jacquemin, Q. Peng, Z. Shuai and D. Escudero, *J. Phys. Chem. C*, 2018, **122**, 6340–6347.
40 K. Veys and D. Escudero, *J. Phys. Chem. A*, 2020, **124**, 7228–7237.
41 Y. Niu, Q. Peng, C. Deng, X. Gao and Z. Shuai, *J. Phys. Chem. A*, 2010, **114**, 7817–7831.
42 R. Kawagoe, I. Takashima and S. Uchinomiya, *et al.*, *Chem. Sci.*, 2017, **8**, 1134–1140.
43 N. A. Shekhovtsov and M. B. Bushuev, *J. Phys. Chem. Lett.*, 2025, **16**, 9152–9158.
44 J. Wei, Y. Wu, R. Pu, L. Shi, J. Jiang, J. Du, Z. Guo, Y. Huang and W. Liu, *J. Phys. Chem. Lett.*, 2021, **12**, 4466–4473.
45 W. Kohn, A. D. Becke and R. G. Parr, *J. Phys. Chem.*, 1996, **100**, 12974–12980.
46 T. Ziegler, *Chem. Rev.*, 1991, **91**, 651–667.
47 Y. Zhao and D. G. Truhlar, *Theor. Chem. Acc.*, 2008, **120**, 215–241.
48 F. Weigend and R. Ahlrichs, *Phys. Chem. Chem. Phys.*, 2005, **7**, 3297–3305.
49 F. Weigend, *Phys. Chem. Chem. Phys.*, 2006, **8**, 1057–1065.
50 A. V. Marenich, C. J. Cramer and D. G. Truhlar, *J. Phys. Chem. B*, 2009, **113**, 6378–6396.
51 J. Tomasi, B. Mennucci and R. Cammi, *Chem. Rev.*, 2005, **105**, 2999–3094.
52 E. Cancès, B. Mennucci and J. Tomasi, *J. Chem. Phys.*, 1997, **107**, 3032–3041.
53 B. Mennucci, E. Cancès and J. Tomasi, *J. Phys. Chem. B*, 1997, **101**, 10506–10517.
54 E. Cancès and B. Mennucci, *J. Math. Chem.*, 1998, **23**, 309–326.
55 J.-D. Chai and M. Head-Gordon, *Phys. Chem. Chem. Phys.*, 2008, **10**, 6615–6620.
56 A. Petersson, A. Bennett, T. G. Tensfeldt, M. A. Al-Laham, W. A. Shirley and J. Mantzaris, *J. Chem. Phys.*, 1988, **89**, 2193–2218.
57 G. Petersson and M. A. Al-Laham, *J. Chem. Phys.*, 1991, **94**, 6081–6090.
58 T. Yanai, D. P. Tew and N. C. Handy, *Chem. Phys. Lett.*, 2004, **393**, 51–57.
59 E. Runge and E. K. Gross, *Phys. Rev. Lett.*, 1984, **52**, 997.
60 R. Bauernschmitt and R. Ahlrichs, *Chem. Phys. Lett.*, 1996, **256**, 454–464.

61 F. Furche and R. Ahlrichs, *J. Chem. Phys.*, 2002, **117**, 7433–7447.
62 M. Caricato, B. Mennucci, J. Tomasi, F. Ingrosso, R. Cammi, S. Corni and G. Scalmani, *J. Chem. Phys.*, 2006, **124**, 124520.
63 M. J. Frisch, G. W. Trucks, H. B. Schlegel, G. E. Scuseria, M. A. Robb, J. R. Cheeseman, G. Scalmani, V. Barone, G. A. Petersson, H. Nakatsuji, X. Li, M. Caricato, A. V. Marenich, J. Bloino, B. G. Janesko, R. Gomperts, B. Mennucci, H. P. Hratchian, J. V. Ortiz, A. F. Izmaylov, J. L. Sonnenberg, D. Williams-Young, F. Ding, F. Lipparini, F. Egidi, J. Goings, B. Peng, A. Petrone, T. Henderson, D. Ranasinghe, V. G. Zakrzewski, J. Gao, N. Rega, G. Zheng, W. Liang, M. Hada, M. Ehara, K. Toyota, R. Fukuda, J. Hasegawa, M. Ishida, T. Nakajima, Y. Honda, O. Kitao, H. Nakai, T. Vreven, K. Throssell, J. A. Montgomery, Jr., J. E. Peralta, F. Ogliaro, M. J. Bearpark, J. J. Heyd, E. N. Brothers, K. N. Kudin, V. N. Staroverov, T. A. Keith, R. Kobayashi, J. Normand, K. Raghavachari, A. P. Rendell, J. C. Burant, S. S. Iyengar, J. Tomasi, M. Cossi, J. M. Millam, M. Klene, C. Adamo, R. Cammi, J. W. Ochterski, R. L. Martin, K. Morokuma, O. Farkas, J. B. Foresman and D. J. Fox, *Gaussian 16 Revision B.01*, Gaussian Inc., Wallingford CT, 2016.
64 D. Mester, P. R. Nagy and M. Kállay, *J. Chem. Phys.*, 2017, **146**, 194102.
65 T. H. Dunning Jr, *J. Chem. Phys.*, 1989, **90**, 1007–1023.
66 C. Angeli, R. Cimiraglia, S. Evangelisti, T. Leininger and J.-P. Malrieu, *J. Chem. Phys.*, 2001, **114**, 10252–10264.
67 C. Angeli, R. Cimiraglia and J.-P. Malrieu, *Chem. Phys. Lett.*, 2001, **350**, 297–305.
68 C. Angeli, R. Cimiraglia and J.-P. Malrieu, *J. Chem. Phys.*, 2002, **117**, 9138–9153.
69 C. Kollmar, K. Sivalingam, Y. Guo and F. Neese, *J. Chem. Phys.*, 2021, **155**, 234104.
70 V. Barone and M. Cossi, *J. Phys. Chem. A*, 1998, **102**, 1995–2001.
71 M. Ceriotti, G. Bussi and M. Parrinello, *Phys. Rev. Lett.*, 2009, **102**, 020601.
72 M. Ceriotti, G. Bussi and M. Parrinello, *J. Chem. Theory Comput.*, 2010, **6**, 1170–1180.
73 A. Prlj, E. Marsili, L. Hutton, D. Hollas, D. Shchepanovska, D. R. Glowacki, P. Slavíek and B. F. E. Curchod, *ACS Earth Space Chem.*, 2022, **6**, 207–217.
74 A. Prlj, D. Hollas and B. F. E. Curchod, *J. Phys. Chem. A*, 2023, **127**, 7400–7409.
75 gle4md: Generalized Langevin Equations for Molecular Dynamics, https://gle4md.org/.
76 D. Hollas, J. Suchan, M. Oncoák, O. Svoboda and P. Slavícek, *ABIN*, 2021, https://github.com/PHOTOX/ABIN.
77 F. Neese, *Wiley Interdiscip. Rev.:Comput. Mol. Sci.*, 2022, **12**, e1606.
78 P. Chakraborty, R. C. Couto and N. H. List, *J. Phys. Chem. A*, 2026, **130**, 1090–1103.
79 S. Hirata and M. Head-Gordon, *Chem. Phys. Lett.*, 1999, **314**, 291–299.
80 D. Mester, P. R. Nagy, J. Csóka, L. Gyevi-Nagy, P. B. Szabó, R. A. Horváth, K. Petrov, B. Hégely, B. Ladóczki and G. Samu, *et al.*, *J. Phys. Chem. A*, 2025, **129**, 2086–2107.
81 M. Kállay, P. R. Nagy, D. Mester, L. Gyevi-Nagy, J. Csóka, P. B. Szabó, Z. Rolik, G. Samu, B. Hégely, B. Ladóczki, K. Petrov, J. Csontos, Á. Ganyecz, I. Ladjánszki, L. Szegedy, M. Farkas, P. D. Mezei, R. A. Horváth and B. D. Lörincz, Mrcc, a quantum chemical program suite written by see https://www.mrcc.hu.
82 A. D. Laurent and D. Jacquemin, *Int. J. Quantum Chem.*, 2013, **113**, 2019–2039.
83 D. Jacquemin, A. Planchat, C. Adamo and B. Mennucci, *J. Chem. Theory Comput.*, 2012, **8**, 2359–2372.
84 A. Dreuw, J. L. Weisman and M. Head-Gordon, *J. Chem. Phys.*, 2003, **119**, 2943–2946.
85 Z.-L. Cai, M. J. Crossley, J. R. Reimers, R. Kobayashi and R. D. Amos, *J. Phys. Chem. B*, 2006, **110**, 15624–15632.
86 C. Halsey-Moore, P. Jena and J. T. McLeskey Jr, *Comput. Theor. Chem.*, 2019, **1162**, 112506.
87 É. Brémond, A. Ottochian, Á. J. Pérez-Jiménez, I. Ciofini, G. Scalmani, M. J. Frisch, J. C. Sancho-García and C. Adamo, *J. Comput. Chem.*, 2021, **42**, 970–981.
88 D. Jacquemin, E. A. Perpete, I. Ciofini, C. Adamo, R. Valero, Y. Zhao and D. G. Truhlar, *J. Chem. Theory Comput.*, 2010, **6**, 2071–2085.
89 M. Barbatti, J. Paier and H. Lischka, *J. Chem. Phys.*, 2004, **121**, 11614–11624.
90 W. J. Glover, T. Mori, M. S. Schuurman, A. E. Boguslavskiy, O. Schalk, A. Stolow and T. J. Martnez, *J. Chem. Phys.*, 2018, **148**, 164303.
91 P. Chakraborty, Y. Liu, T. Weinacht and S. Matsika, *J. Chem. Phys.*, 2020, **152**, 174302.
92 P. Chakraborty, R. C. Couto and N. H. List, *J. Phys. Chem. A*, 2023, **127**, 5360–5373.
93 S. Athanasopoulos, L. Alfonso Hernandez, D. Beljonne, S. Fernandez-Alberti and S. Tretiak, *J. Phys. Chem. Lett.*, 2017, **8**, 1688–1694.

